Available online at www.sciencedirect.com
ScienceDirect
Bioelectrochemistry 70 (2007) 71–77
Bioelectrochemistry
www.elsevier.com/locate/bioelechem

Nonlinear current–voltage relationship of the plasma membrane of single CHO cells

Henning Krassen [a], Uwe Pliquett [a,b], Eberhard Neumann [a,*]

[a] *Faculty of Chemistry, University of Bielefeld, D-33615-Bielefeld, Germany*
[b] *Center for Bioelectrics, Old Dominion University, Norfolk, VA 23510, USA*

Received 10 June 2005
Available online 7 April 2006

Abstract

The application of electric field pulses to Chinese Hamster Ovary (CHO) cells causes membrane electroporation (MEP). If a voltage or current ramp is applied to the cellular membrane of a single CHO cell, the membrane conductance increases nonlinearly with field strength reaching saturation. In particular, the kinetics of the induced conductance changes represents the data basis for the interpretation in terms of underlying structural changes. The current/voltage characteristic is found to be continuous, but displays occasionally a sharp increase in the conductance. The step-like increases are interpreted to reflect the formation of one (or more) larger pore(s). The analysis of current clamp data yields pores of radius (r_p) in the range of $2.5 \le r_p/\mathrm{nm} \le 20$; the pores of the voltage clamp data are in the range of $2.5 \le r_p/\mathrm{nm} \le 55$. The larger pores occur predominantly during hyperpolarising and less frequently during depolarising conditions, respectively. The different kinetics of pore formation in the hyperpolarising condition, where the inward field increases, and the depolarising condition, where the inward field first decreases and then increases in the opposite direction, suggests structural asymmetry with respect to the direction of the electric membrane field. At the required higher voltage, the effect of the resting potential is negligibly small.

Keywords: Membrane electroporation; Single cell configuration; Whole cell clamp; Large pores; Current/voltage characteristics

1. Introduction

The lipid bilayer membrane is functionally an effective barrier for the transport of small ions and polyions, like DNA. Non-polar and small-polar molecules like water can diffusively penetrate and cross the lipid phase of membranes. Membrane electroporation (MEP) renders cellular and artificial lipid membranes transiently permeable to all types of molecules. The seminal early example for the first functional electrotransfer of naked DNA to suspended cells [1], already provides basic information useful for optimisation strategies in the new medical disciplines of electrogenetherapy and electrochemotherapy [2,3]. Another fruitful application of MEP is the enhancement of transdermal drug transport. Here it is the *stratum corneum* of the skin which is effectively permeabilized by MEP [4].

Originally, the concept and methodology of MEP received great attention in cell biology and biotechnology. The scientific discipline of biophysics has used MEP as a research tool for providing guidelines for the efficient control of goal-directed manipulations of organelles and cells [5]. As a new approach, we use here the whole-cell clamp technique (WCC) and apply, respectively, depolarising and hyperpolarising electric field pulses to the plasma membrane of a single cell. The WCC-configuration is different to conventional set ups for MEP of cells, organelles and lipid vesicles in suspensions, where effectively only the pole cap areas of the spherical shell objects are electroporated during one pulse. In the WCC configuration [6], the entire membrane is identically exposed to the same electric field strength. The direction of the natural membrane field of a CHO cell, corresponding to a negative membrane potential, is from the outside to the inside of the cell.

The increase in the electrical conductance caused by MEP is usually interpreted to reflect an increase of the number of pores within the lipid bilayer part of the membrane [1,4–6,8]. In the

* Corresponding author. Tel.: +49 521 106 2053; fax: +49 521 106 2981.
E-mail address: eberhard.neumann@uni-bielefeld.de (E. Neumann).

1567-5394/$ - see front matter © 2006 Elsevier B.V. All rights reserved.
doi:10.1016/j.bioelechem.2006.03.033

WCC mode, the respective conductance–time curves are calculated from the kinetic data of voltage clamp and current clamp configurations, respectively.

The analysis of the data finally aims at establishing the basis for the optimisation of pulse protocols for biotechnological and biomedical applications. The WCC method, as such, may be used for the electrical characterisation of biological cells. One key result of this study is the perspective that, for cells and cell pellets in the conventional mode of measurement between two planar electrodes, it is the anodic pole cap (hyperpolarised) which is affected more strongly than the cathodic pole cap (depolarised).

1.1. Depolarising and hyperpolarising field pulses

The natural membrane potential $\Delta\varphi_{nat}$ is conventionally defined as the difference between the electric potentials of the cytosolic (inner) side φ_{in} and the extracellular side φ_{out}, according to:

$$\Delta\varphi_{nat} = \varphi_{in} - \varphi_{out}, \quad (1)$$

where in electrophysiology the definition $\varphi_{out}=0$ is used as the reference. In the presence of an externally applied electric field, the total membrane potential $\Delta\varphi_m$ is given by the sum of $\Delta\varphi_{nat}$ and the induced membrane potential $\Delta\varphi_{ind}$:

$$\Delta\varphi_m = \Delta\varphi_{nat} + \Delta\varphi_{ind} \quad (2)$$

Since the membrane field is defined by $E_m = -\Delta\varphi_m/d_m$, Eq. (2) yields:

$$E_m = E_{nat} + E_{ind}, \quad (3)$$

where $E_{nat} = -\Delta\varphi_{nat}/d_m$ and $E_{ind} = -\Delta\varphi_{ind}/d_m$, respectively. In this context, the hyperpolarising pulse mode is specified as:

$$\Delta\varphi_{ind} \le 0; \quad E_{ind} \ge 0 \quad (4)$$

and, respectively, the depolarising pulse mode as:

$$\Delta\varphi_{ind} \ge 0; \quad E_{ind} \le 0 \quad (5)$$

During hyperpolarisation the membrane field E_m increases in the direction of the natural field vector (E_{nat}). During depolarisation the E_m first decreases down to zero and then increases in the opposite direction to the natural field vector (E_{nat}) (see Fig. 1).

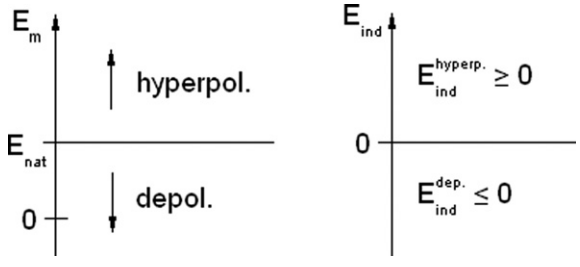

Fig. 1. Hyperpolarisation $\Delta\varphi_{ind} = \Delta\varphi_m - \Delta\varphi_{nat} \le 0$ and depolarisation $\Delta\varphi_{ind} \ge 0$, represented in terms of field strength $E_m = -\Delta\varphi_m/d_m$, respectively.

2. Material and methods

2.1. Single cells

CHO-K1 cells, a subclone of an isolated somatic Chinese hamster ovary (CHO) cell line, is used throughout our experiments. They are cultivated in DMEM/F12 medium containing 5% FCS and 10–100 mg/L of the antibiotics benzyl penicillin and streptomycin sulphate at 310 K (37 °C) in an incubator (5% CO_2). Normally, before use, the cells are washed in buffered 0.15 M KCl, 1 mM HEPES (TMA) solution, pH 7.2 at 296 K (23 °C) and resuspended in buffer. Here, in order to handle undisturbed cells, we use culture medium, pH 8 at 293 K (20 °C) as the external solution for the cell.

2.2. Glass capillaries

Patch glass capillaries (PG120T-7.5 HARVARD Part No. 30-0091) as well as borosilicate glass capillaries (GC120T-7,5 HARVARD Part No. 30-0049) have been used. Both have an outer diameter of 1.2 mm and an inner diameter of 0.93 mm (resp. 0.94 mm).

A DMZ-Universal Microelectrode Puller (Zeitz, Munich, Germany) is used to produce tip diameters between 2 and 3.5 μm. The resistance of the pipette filled with culture medium is between 2 and 3.5 MΩ.

2.3. Measurement chamber

The central part of the measuring chamber contains the culture medium in which the single cell is placed [6,7]. The measuring temperature is 296 K (23 °C). An Ag/AgCl electrode is fixed on the inner wall of the chamber. The second electrode is inside the mobile pipette filled with medium. The tip of the pipette is located near the cell surface. A liquid flow is initiated by careful reducing the pressure inside the pipette. The cell attaches to the tip and a connection between cytosol and the second electrode is established. The attachment quality is controlled by video microscopy and verified by measuring the resistance.

2.4. Microscope

A phase contrast microscope (Olympus CH-2) with a 63× water immersion objective (ZEISS 1036-024 chropla 63×/0.95W Ph3 ∞/0) is equipped with a CCD camera (Panasonic WV-BP100/G) for monitoring the cell during the experiments.

The videos have been captured with full frame rate (50 fps, DVnov video capture card) for further processing.

2.5. Arbitrary function generator

The microcontroller-based device is generating waveforms up to 10 s with a temporal resolution of 500 μs. Using proper feedback, the voltage across the membrane or the total current has been controlled with 12-bit resolution. The applied voltage is in the range $-10 \le U/V \le +10$; the current is controlled in the range $-350 \le I/nA \le +350$. A higher resolution of smaller voltage and

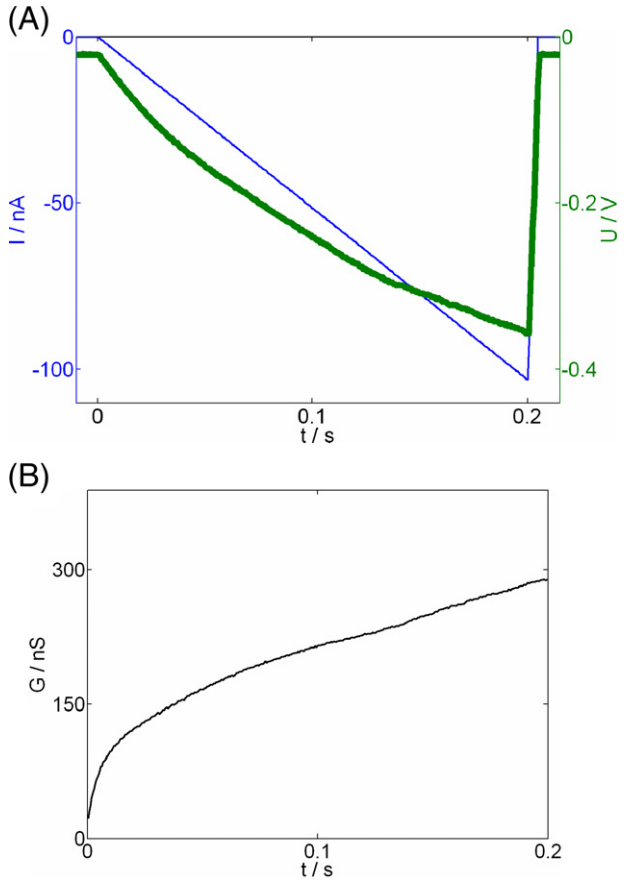

Fig. 2. (A) Voltage (bold line), $U(t)$, as the response to a current ramp (thin line) $I(t)$, during hyperpolarisation of the plasma cell membrane of a single CHO cell, bathed in culture medium at pH 7.4 and 296 K (23 °C) and (B) cell membrane conductance $G(t)=I(t)/U(t)$, as a function of time (t), respectively. The convex appearance of $G(t)$ at the beginning is due to the not fully compensated resting potential of the membrane. The conductance in the absence of the applied (hyperpolarising) voltage is $G=105$ nS.

current is achieved by a feedback gain. The current and voltage is monitored using matching amplifiers and a 12-bit ADC. Electronic compensations are made for the dc-offset and the liquid junction potentials, using the generalised Henderson equation. The device consists of a headstage with the matching amplifiers and a basic station connected to a PC. All programming at the PC is in MATLAB; the basic device is programmed in ASSEMBLER. The entire apparatus, including the microscope, is mounted on a stone plate for acoustic damping and is surrounded by a faraday cage for electrical shielding.

All experimental traces are monitored by video microscopy. For synchronisation of the video with the electrical measurements we use the audio-channels, one for recording the electrical signal and the other one for recording the frame synchronisation signal of the video. Further on, the highly automated processing of the video sequences is programmed in MATLAB.

2.6. Pulse protocols

The shape of the applied pulses is chosen according to the parameters tested. The current/voltage characteristic of the plasma membrane of a single cell is derived from ramp functions. Rectangular pulses are applied when we aim at the relaxation kinetic parameters at a constant membrane field.

In order to estimate the field strength range of MEP, it is appropriate to control the current rather than the voltage. For the kinetics of pore formation at a given field strength, the voltage is controlled. Note that it is the voltage across the plasma membrane rather than the voltage across the pipette. This control is accomplished by a feedback circuitry, applying an equivalent circuit for the pipette. Prior to the actual experiment, in each case the equivalent circuit is adjusted to the behaviour of the individual pipette.

In the experiments, the polarity of the pulses (negative for hyperpolarisation and positive for depolarisation), the voltage/current function and the stimulus/time—function (ramp slope, pulse duration) are varied, respectively. Before and after each pulse, the impedance spectrum is measured using a time domain approach with a rectangular wave (100 Hz) as stimulus for 0.5 s (before) and 6.2 s (after), respectively.

3. Results

The aim has been to characterise the electroporated plasma membrane of a single cell under stationary conditions, where induced pore formation and resealing have the same rate. For our working conditions, the natural current sources from ionic

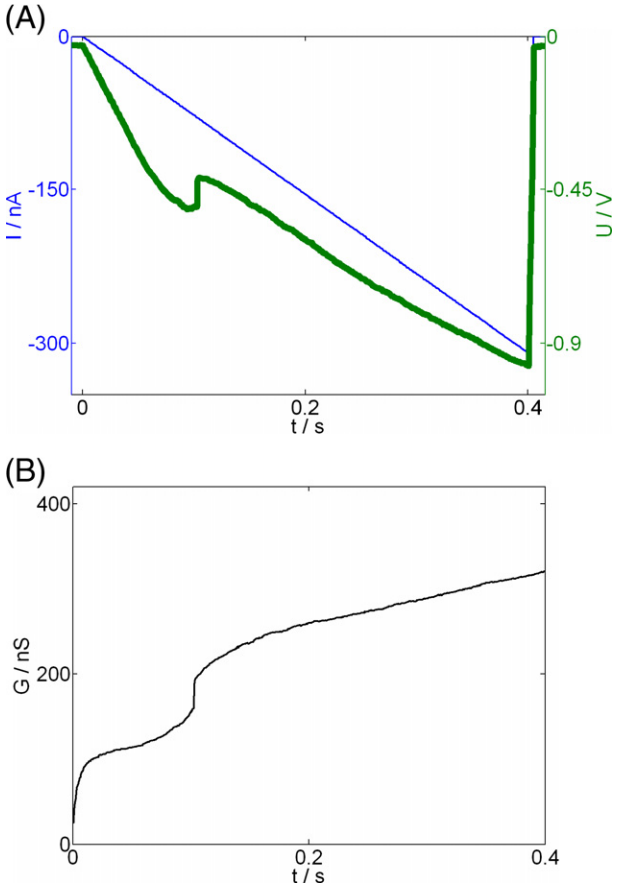

Fig. 3. (A) Distinct step in voltage (bold), at 100 ms, during current (thin) controlled stimulus $I(t)$. (B) Membrane conductance $G(t)=I(t)/U(t)$ showing a sharp increase at 100 ms. For experimental conditions, refer to Fig. 2.

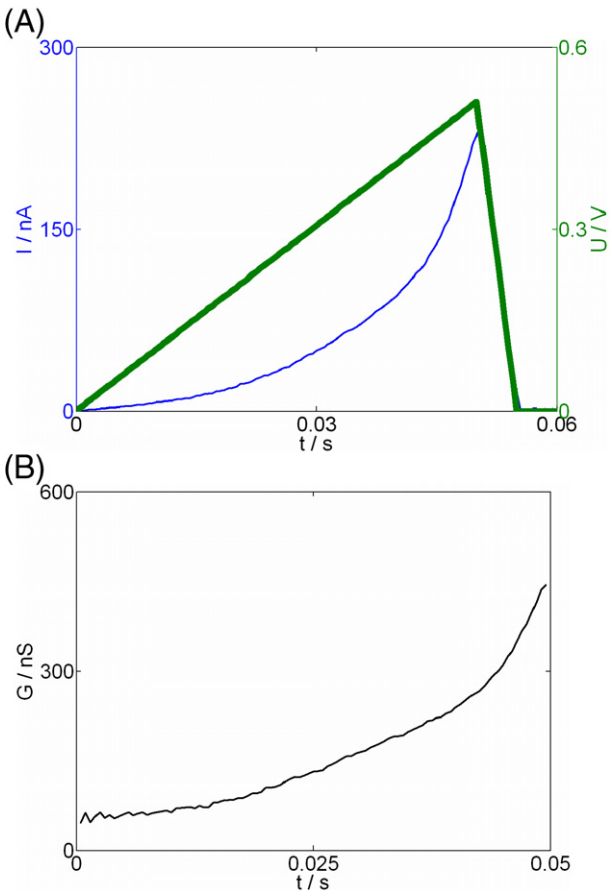

Fig. 4. (A) Current (thin line) $I(t)$ as the response to a voltage ramp (thick line) $U(t)$, applied to the plasma cell membrane of a single CHO cell, bathed in culture medium at pH 7.4 and 296 K (23 °C), during a depolarising voltage clamp configuration and (B) the respective calculated conductance $G(t)=I(t)/U(t)$ as a function of time, respectively.

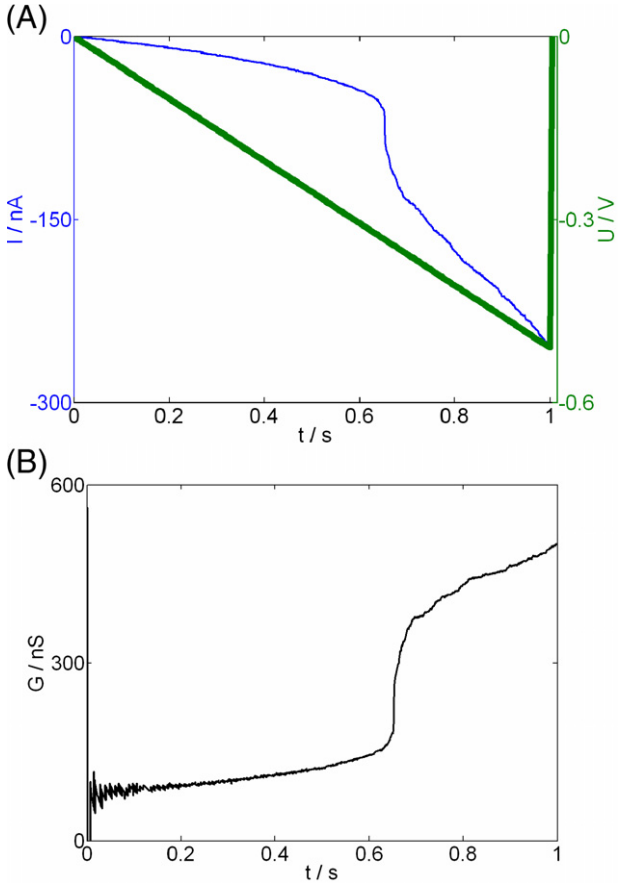

Fig. 5. (A) Sharp decrease in the current (thin line) $I(t)$ and (B) calculated membrane conductance $G(t)=I(t)/U(t)$, respectively, at the time $t=0{,}65$ s, during hyperpolarising voltage (thick line) clamp, $U(t)$. For experimental conditions, see the legend to Fig. 4.

channel proteins and pump proteins of the living cells are negligibly small compared to the clamp-induced currents. In CHO cells, the short circuit current of the plasma membrane is about 3 nA, which is significantly below the current stimulus, which is between −404 and +404 nA. Thus, only the initial stimulated currents and voltages are slightly distorted by the natural ones, respectively. Fig. 2 shows that the conductance continuously increases with increasing current in current clamp configuration. This is interpreted as reflecting the formation of an increasing number of small conductive pores.

While the stimulus $I(t)$ increases, there is occasionally a sharp decrease in voltage U_m (Fig. 3), equivalent to a decrease in the membrane field strength $E_m=U_m/d_m$, where $d_m\approx 10$ nm is the estimated plasma membrane thickness. Such a sharp step of current increase, and thus conductance increase, occurs in about 40% of the measurements, suggesting the occasional creation of one (or more) larger pore(s) probably at the expense of smaller pores.

In voltage clamp experiments (Figs. 4 and 5), the continuous part of the current and conductance traces similarly reflects an increasing number of small pores as a response to both, hyperpolarisation as well as to depolarisation, because the contribution of $\Delta\varphi_{nat}$ is negligibly small.

The data show that under hyperpolarising conditions the probability of appearance of occasional step-like jumps is significantly higher than under depolarising conditions.

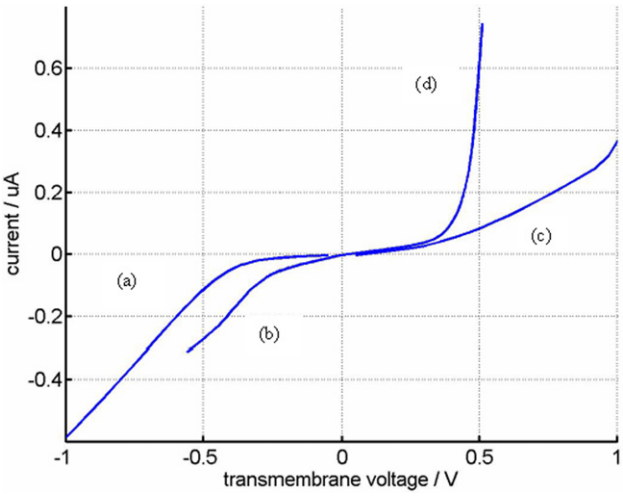

Fig. 6. Current–voltage characteristics at two different negative and positive ramp slopes, respectively: v_r/(V/s)=−1 (a), −0.01 (b), +0.1 (c), +0.01 (d). At $v_r=1$ V/s, instantaneous breakdown (rupture) of the membrane occurs. A new cell is used for each ramp stimulus.

It is found that the current–voltage relationship is highly dependent on the slope of the voltage ramp (Fig. 6). A larger slope of the voltage ramp causes a larger conductance slope. Therefore, the voltage $U_m = E_m \cdot d_m$ across the membrane is higher for current stimuli with higher slope; reaching, for instance, the value of $\Delta\varphi = -1.5$ V for the slope rate $v_r = 100$ V/s.

4. Discussion

The clamp-induced conductance changes in the plasma membrane of single CHO cells clearly reflect MEP. Electrothermodynamically, MEP is described in terms of structural transitions from closed (C) to porated (P) membrane states, according to: (C)⇌(P). For densely packed cell pellets, the minimum reaction scheme for MEP of CHO cell pellets is a three-step reaction cascade between two (closed) prepore states and two types of (open) pore states [8]. A part of the current, voltage and conductance traces obtained for single cells (Figs. 2 and 4) can be interpreted along a similar reaction scheme.

In the particular examples of Figs. 3 and 5, 52% of the current clamp and 39% of the voltage clamp data, the conductance occasionally shows a step-like increase, at random times, during pulse application. These sharp conductance changes are interpreted as the formation of one (or more) larger pore(s). This behaviour may be compared with reports [9] on the pore kinetics

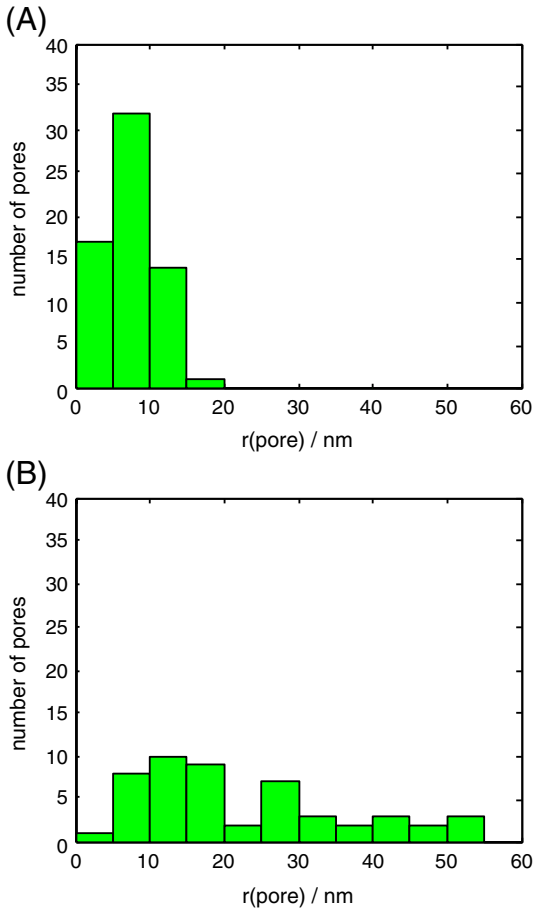

Fig. 7. Histogram of the number of pores with the radius r (A) during current clamp and (B) during voltage clamp, respectively, of single CHO cells.

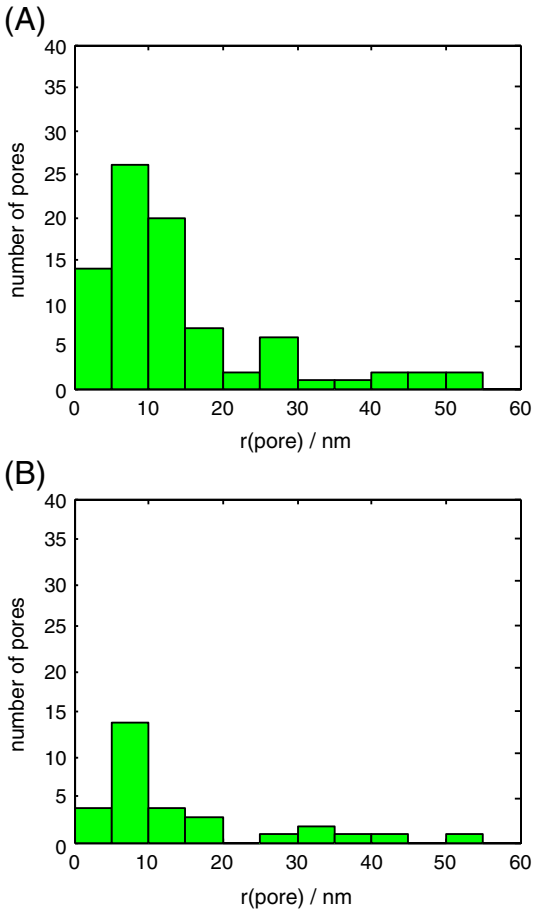

Fig. 8. Histogram of the number of pores with the radius r (A) during hyperpolarisation and (B) during depolarisation, respectively, of single CHO cells.

in tense planar lipid bilayer membranes (BLM), where the formation of a larger pore starts as a singular event, leading finally to irreversible electrical breakdown (rupture). The sharp conductance steps in the otherwise continuous conductance changes of cellular membranes [5–10], studied here, however, cannot be compared with the electrical behaviour of the BLM.

A lipid membrane may be physically approximated as a two-dimensional fluid system, where the lipid bilayer configuration is held together by the polar solvent water. The irreversible breakdown of the artificial BLM in an externally applied voltage is essentially caused by preponderance of the outer tension exerted by the lipid torus, a component which is missing at cellular membranes. It appears that, in a planar BLM, once one of the induced smaller pores exceeds a critical size, it finally leads to mechanical rupture.

In partially supported lipid bilayers or lipid/protein membranes, the interacting forces can be quite different. A cellular plasma membrane spans over the supporting scaffolding of, for instance, spectrins, connected with integrins and actin complexes. It is only with respect to the tension that the curved plasma membrane may be compared with a tense BLM rather than with a curved lipid vesicle membrane.

The plasma membrane, anchored to external and internal supporting sites, is under additional strain and stress, where

cytoskeleton elements appear to contribute to a kind of inner membrane tension. The membrane appears overall stable and relaxed after the formation of one (or more) larger pore(s). The formation of larger pores appears to occur, spontaneously, from initially smaller electropores. The probability of the formation of larger pores is increased at higher field strength. The probability distribution of the occurrence of a larger pore (Figs. 7 and 8), however, presently cannot be quantified.

4.1. Calculation of the pore radius in the single pore model

The pore radius r_p of a cylindrical pore of area A_p and thickness d_m is calculated from the step-like increase in the conductance, viewed as the formation of one single larger pore. The pore resistance R_P is viewed as the sum $R_P = R_I + R_S$. R_I is the resistance of the pore itself while R_S is the spreading resistance due to the deformation of field lines around a pore within the bulk medium. While for small pores ($r_p < 1$ nm) the spreading resistance is negligibly small, it is increasingly important for larger pores. For a cylindrical pore, R_I is calculated according to:

$$R_I = \frac{1}{\sigma} \cdot \frac{d_m}{A_p} = \frac{1}{\sigma} \cdot \frac{d_m}{\pi \cdot r_p^2} \tag{6}$$

where σ is the conductivity of the liquid inside the pore. The differential change dR_S of R_S is given by:

$$dR_S = 2 \cdot \frac{1}{\sigma} \cdot \frac{dx}{A_p} = \frac{1}{\sigma} \cdot \frac{dx}{\pi \cdot x^2}, \tag{7}$$

where x is the distance to the membrane surface. Integration within the boundaries $x = r_p$ and $x = \infty$, yields:

$$R_S = \frac{1}{\pi\sigma} \cdot \int_{r_p}^{\infty} \frac{1}{x^2} dx = \frac{1}{\pi\sigma} \cdot \left(\frac{1}{r_p} - \frac{1}{\infty} \right) = \frac{1}{\pi\sigma} \cdot \frac{1}{r_p}, \tag{8}$$

Inserting Eqs. (4) and (6) into the expression for the pore resistance $R_P = R_I + R_S$, yields:

$$R_P = \frac{1}{\sigma} \cdot \frac{d_m}{\pi \cdot r_p^2} + \frac{1}{\pi \cdot \sigma} \cdot \frac{1}{r_p}, \tag{9}$$

where we may assume that the pore interior is bath medium. The measured conductivity is $\sigma_{Medium} = 15.2$ mS/cm and is set equal to σ.

4.2. Statistical distribution of larger pores

The number of larger pores caused by MEP under current clamp conditions is relatively small (Fig. 7(A)); about 98% of the pores are in the range of $1 \le r/\text{nm} \le 15$.

Using Ohm's law, an increase in conductance at constant current results in a definite decrease of the voltage U_m, and thus of the field strength $E_m = U_m \cdot d_m$. The enlargement of pores in the current-controlled configuration (current clamp) appears to be a self-inhibiting process. The number of larger pores formed during electroporation under voltage clamp conditions is even greater (see Fig. 7(B)); where about 62% of the pores are in the range of $15 \le r/\text{nm} \le 55$. It is recalled that the sharp increase in the conductance results from MEP at constant voltage, where apparently the enlargement of pores is a self-enforcing process.

The largest pore in the single-pore assumption, calculated from the largest step, has a radius $r = 55$ nm. This upper limiting value is in the same order of magnitude as the average linear distance between the cytoskeleton elements touching the inner surface of the plasma membrane [11]. Thus, the structure of the cytoskeleton appears to determine the largest radius of the electrically induced pores by supporting the membrane and thus preventing mechanical rupture. The spectrin mesh appears to limit further increase in the pore size.

A significant higher probability of appearance of larger pores at hyperpolarisation conditions, as compared to depolarisation, is evident in Fig. 8. There is, however, no difference in the distribution of pore size at comparable field strengths.

Since CHO-cells are not excitable, voltage-gated channels appear not to be involved. A probable origin of the electrical asymmetry is the asymmetry of the membrane. In cellular membranes, some types of lipids are predominantly found in the cytosolic layer, others in the extracellular one. The field effect on the lipids obviously depends on the local field strength and the field direction. Such an asymmetry may account for a sidedness due to different lipid composition in the two layers of the lipid bilayer parts of plasma membranes.

4.3. Conclusion

The electrically induced larger pores are apparently the local membrane structures which appear to be involved in the electrically mediated uptake of large molecules like DNA or anticancer drugs by the cells under voltage or current clamp conditions, respectively. The formation of larger pores is also a key information for optimisation strategies to efficiently electrotransfer drugs and DNA into cells. Interestingly, the current and voltage parameters are the same for conductive (voltage clamp) and for non-conductive (current clamp) media, surrounding the plasma membranes.

Acknowledgements

We gratefully acknowledge financial support by the DFG, Bonn/Bad Godesberg for grant No. 227/9-3, /9-4 and the European Union, Brussels, for grant QLK3-CT-1999-00484 to E.N.

References

[1] E. Neumann, M. Schaefer-Ridder, Y. Wang, P.H. Hofschneider, Gene transfer into mouse lyoma cells by electroporation in high electric fields, EMBO J. 1 (1982) 841–845.
[2] S. Orlowski, L. Mir, Cell electropermeabilisation: a new tool for biochemical and pharmacological studies, Biochim. Biophys. Acta 1154 (1993) 51–63.
[3] J. Belehradek Jr., S. Orlowski, L. Ramirez, G. Pron, B. Poddevin, L. Mir, Electropermeabilization of cells in tissues assessed by the qualitative and quantitative electroloading of bleomycin, Biochim. Biophys. Acta, Biomembr. 1190 (1994) 155–163.
[4] U. Pliquett, J.C. Weaver, Electroporation of human skin: simultaneous measurement of changes in the transport of two fluorescent molecules and

in the passive electrical properties, Bioelectrochem. Bioenerg. 39 (1996) 1–12.
[5] E. Neumann, K. Rosenheck, Permeability changes induced by electric impulses in vesicular membranes, J. Membr. Biol. 10 (1972) 279–290.
[6] C.G. Frantescu, D. Wesner, U. Pliquett, E. Neumann, Unsymmetrical non-linearity in cell membranes, Proceedings of the XII International Conference on Electrical Bioimpedance, Gdansk (PL), 2004, pp. 41–44.
[7] C.G. Frantesu, U. Pliquett, E. Neumann, The membrane impedance before and after electroporation of single Chinese Hamster Ovary cells, Proceedings of the 12th Heiligenstädter Kolloquium, Heiligenstadt, 2004, pp. 217–224.
[8] M. Schmeer, T. Seipp, U. Pliquett, S. Kakorin, E. Neumann, Mechanism for the conductivity changes caused by membrane electroporation of CHO cell-pellets, Phys. Chem. Chem. Phys. 6 (2004) 5564–5574.
[9] C. Wilhelm, M. Winterhalter, U. Zimmermann, R. Benz, Kinetics of pore size during irreversible electrical breakdown of lipid bilayer membranes, Biophys. J. 64 (1993) 121–128.
[10] A. Barnett, J.C. Weaver, Electroporation: a unified, quantitative theory of reversible electrical breakdown and mechanical rupture in artificial planar bilayer membranes, Bioelectrochem. Bioenerg. 25 (1991) 163–182.
[11] T. Byers, D. Branton, Visualisation of the protein associations in the erythrocyte membrane skeleton, Proc. Natl. Acad. Sci. U. S. A. 82 (1985) 6153–6157.